Classical dipoles on the kagome lattice

Mykola Maksymenko,[1,2,*] V. Ravi Chandra,[3] and Roderich Moessner[1]
[1]*Max-Planck-Institut für Physik komplexer Systeme, Nöthnitzer Straße 38, 01187 Dresden, Germany*
[2]*Department of Condensed Matter Physics, Weizmann Institute of Science, Rehovot 76100, Israel*
[3]*School of Physical Sciences, National Institute of Science Education and Research, Institute of Physics Campus, Bhubaneswar 751005, India*
(Received 21 February 2015; revised manuscript received 18 April 2015; published 15 May 2015)

Motivated by recent developments in magnetic materials, frustrated nanoarrays, and cold atomic systems, we investigate the behavior of dipolar spins on the frustrated two-dimensional kagome lattice. By combining the Luttinger-Tisza approach, numerical energy minimization, spin-wave analysis, and parallel tempering Monte Carlo, we study long-range ordering and finite-temperature phase transitions for a Hamiltonian containing both dipolar and nearest-neighbor interactions. For antiferromagnetic exchange and both weak and moderate dipolar interactions, the system enters a three-sublattice long-range ordered state with each triangle having vanishing dipole and quadrupole moments; whereas for dominating dipolar interactions we uncover ferrimagnetic three-sublattice order. These are also the ground states for XY spins. We discuss excitations of, as well as phase transitions into, these states. We find behavior consistent with Ising criticality for the 120° state, whereas the ferrimagnetic state appears to be associated with drifting exponents. The celebrated flat band of zero-energy excitations of the kagome nearest-neighbor Heisenberg model is lifted to finite energies but acquires only minimal dispersion as dipolar interactions are added.

DOI: 10.1103/PhysRevB.91.184407 PACS number(s): 75.10.Hk, 75.30.Ds, 75.40.Mg

I. INTRODUCTION

Long-ranged dipolar interactions occur in any lattice system of interacting magnetic moments. However, the assessment of the relevance of dipolar interactions in determining the behavior of magnetic systems has witnessed a recalibration in the recent past. This is largely due to the advent of several experimental systems that shifted the focus away from purely exchange-coupled magnets where the dipolar interaction is routinely neglected.

We can identify at least three broad classes of systems which have led to this renewed interest in dipolar interactions. The first are the $A_2B_2O_7$ pyrochlore oxides, which most closely resemble conventionally studied magnetic systems [1]. For these, as a result of an interplay of crystal-field effects, geometry, and the specific magnetic ions involved, the dipolar interactions can be appreciable. A second class is that of nanomagnetic arrays [2], collections of nanomagnetic islands arranged in a regular pattern using lithography. The magnitude of the moments as well as the strength of the dipolar interactions can be tuned to a great degree by controlling the dimensions and separation of the magnetic islands. These systems are much more tunable than the thin-film systems studied in the past with a view to analyzing pattern formation and ordering via the dipolar interaction [3]. Finally, the past decade has seen rapid development of magnetic systems of polar molecules and atomic gases with large dipole moments confined in optical lattices [4,5].

Of particular interest is the interplay of dipolar interactions and geometrical frustration. On frustrated lattices, an exchange term typically gives rise to a macroscopically degenerate yet locally strongly constrained ground-state manifold, usually lacking conventional magnetic order. This constraint can be thought of as restricting the space of states, often in a topologically nontrivial way, within which dipolar interactions are to be minimized; or, conversely, the dipolar interactions can be thought of as lifting the degeneracy, akin to the usual order-by-disorder physics characteristic of quantum and thermal fluctuations [6]. The combination of exchange and dipoles can lead to surprising results, such as in the case of spin ice [7] where the underlying elementary excitations can be seen as doubly gauge charged [8] (emergent) magnetic monopoles [9].

Theoretical efforts to study dipolar spins are several decades old [10–13]. An early milestone is the work of Luttinger and Tisza (LT) [10] who established that the ground state for a simple cubic lattice of dipoles is an antiferromagnetic arrangement of chains of aligned dipoles. Thereafter, Maleev [13] found that the long-range and anisotropic nature of the dipolar interactions can stabilize long-range order in two-dimensional (2D) magnets—something that is prohibited for short-ranged isotropic exchange Hamiltonians because of the Mermin-Wagner theorem. Indeed, for nanomagnetic arrays and cold atoms in optical lattices the study of two dimensions is particularly relevant. For dipoles on the square lattice the ground state likely consists of antiferromagnetically aligned ferromagnetic legs [14,15] and closely related degenerate states [16]. For the triangular lattice a ferromagnetic phase has been reported for purely dipolar interactions, but it was argued that other phases, such as a 120° phase and striped antiferromagnetic phases appear for increasing strength of the exchange interaction [17–20]. Although there is some agreement about the nature of the low-temperature phase for several of these systems the precise details of the transition to those low-temperature phases are frequently under debate. The principal reason lies in the subtleties involved in the thermodynamic limit in the presence of long-ranged (and anisotropic) interactions.

*mykola.maksymenko@weizmann.ac.il

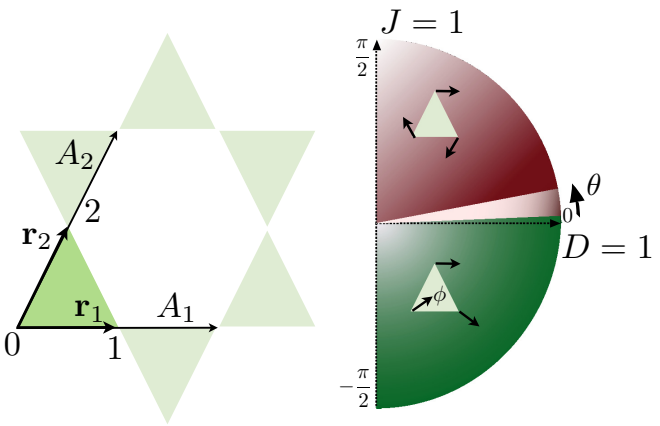

FIG. 1. (Color online) The kagome lattice (left) and the ground-state phase diagram of the model consisting of nearest-neighbor exchange $J = \sin\theta$ and dipolar interactions of strength $D = \cos\theta$ (right). A_1 and A_2 are the basis vectors of the triangular Bravais lattice, and a dark green triangle denotes the unit cell of three sites labeled by $\mathbf{r}_0 = (0,0)$, $\mathbf{r}_1 = (1/2,0)$, and $\mathbf{r}_2 = (0,1/2)$ in this basis. The system exhibits long-range 120° order for $\pi/2 \geqslant \theta > \theta_1$ with $\theta_1 = 10.01°$ and ferrimagnetic order for $-\pi/2 < \theta < \theta_2$ where $\theta_2 = 1.03°$. The latter has two spins inclined with respect to one of the unit-cell edges by angle $\pm\phi(\theta)$. The area between two phases possibly contains an incommensurate intermediate regime.

For some otherwise well-studied lattices, not even the dipolar ground state is known. A case in point is that of classical dipolar spins on the kagome lattice, the focus of this paper. The kagome is perhaps the most-studied two-dimensional highly frustrated lattice for which even the low-temperature behavior of a simple nearest-neighbor Heisenberg model is remarkably intricate [21,22]. We investigate in this paper using a combination of the LT method, spin-wave calculations, numerical energy minimization, and extensive Monte Carlo (MC) simulations the interplay of exchange and dipolar interactions. We find two distinct low-temperature orderings. Starting with antiferromagnetic (AFM) nearest-neighbor exchange, for weak dipolar interactions we observe 120° three-sublattice order with a zero net moment; whereas for strong dipolar interactions we find a peculiar ferrimagnetic state with a continuously varying net moment, which persists also for the case of ferromagnetic (FM) exchange. Thus we have two different three-sublattice $\mathbf{k}_0 = (0,0)$ states at weak and strong dipolar interactions [Fig. 1(b)]. Although our results for the case of strong dipolar interactions predict a finite moment per unit cell as in earlier work [23], our extensive simulations and analytic considerations do not support the existence of a disordered nonmagnetic sublattice.

The outline of the paper is as follows. In Sec. II we introduce the model and conventions used. In Sec. III we present the ground-state phase diagram from the Luttinger-Tisza approach [10]. This method fails in the case of the strong dipolar term, hence in Sec. IV we perform a numerical search for the ground state, and in Sec. V we confirm that this state is locally stable via a spin-wave analysis. Finally, in Sec. VI we analyze our model using a parallel-tempering Monte Carlo method which confirms our predictions for the ground states and provides the details of the corresponding rich finite-temperature phase transitions. We close with a discussion section.

II. MODEL

The kagome lattice given in Fig. 1 is an Archimedean lattice [24], a triangular lattice of triangles. The positions of the triangular Bravais lattice points are denoted by $\mathbf{R}^l$ whereas each site in the unit cell is labeled by $\mathbf{r}_i$ so that a site is labeled by $\mathbf{R}_i^l = (\mathbf{R}^l + \mathbf{r}_i)$. Throughout the paper the lattice constant R_{nn} is set to 1/2 such that the full translation of the three-site unit cell is the unit of length.

The general Hamiltonian of the system of N spins is

$$H = \sum_{k,i,l,j} \sum_{\alpha,\beta} J_{ij}^{\alpha\beta}\left(\mathbf{R}_{ij}^{kl}\right) S_i^{\alpha}(\mathbf{R}^k) S_j^{\beta}(\mathbf{R}^l), \tag{1}$$

$$J_{ij}^{\alpha\beta}(\mathbf{R}) = \frac{1}{2}\left[J\delta_{\alpha\beta,|\mathbf{R}|=R_{nn}} + DR_{nn}^3\left(\frac{\delta_{\alpha\beta}}{|\mathbf{R}|^3} - 3\frac{R^{\alpha}R^{\beta}}{|\mathbf{R}|^5}\right)\right]. \tag{2}$$

Here $\mathbf{R}_{ij}^{kl}$ is the vector between two interacting classical $O(3)$ spins $S_i^{\alpha}(\mathbf{R}^k)$ and $S_j^{\beta}(\mathbf{R}^l)$ of unit length. k and l index the unit cell, whereas i and j run over the sites of the basis in the unit cell and greek α and β denote the components of the vectors x, y, and z. The first term of the interaction matrix (2) is the nearest-neighbor exchange whereas the second is the dipole interaction with R_{nn}^3 as the nearest-neighbor distance, included for normalization. A factor $\frac{1}{2}$ has been included to avoid double counting. $J > 0$ is the energy scale of the antiferromagnetic nearest-neighbor exchange. The dipolar energy scale is

$$D = \frac{\mu_0}{4\pi}\frac{\mu^2}{R_{nn}^3}, \tag{3}$$

where μ is the magnetic moment of the ions.

We parametrize the relative strength of J and D via an angle θ (Fig. 1),

$$J = \sin\theta, \quad D = \cos\theta, \tag{4}$$

with the unit of energy set to $J^2 + D^2 = 1$.

Fourier transformation of the Hamiltonian (2) yields

$$H = \sum_{\mathbf{k},i,j} J_{ij}^{\alpha\beta}(\mathbf{k}) S_i^{\alpha}(-\mathbf{k}) S_j^{\beta}(\mathbf{k}), \tag{5}$$

$$J_{ij}^{\alpha\beta}(\mathbf{k}) = \sum_{kl} J_{ij}^{\alpha\beta}\left(\mathbf{R}_{ij}^{kl}\right) \exp\left[-i\mathbf{k}\mathbf{R}_{ij}^{kl}\right]. \tag{6}$$

We generate the interaction matrix for the dipolar interactions using the Ewald summation [25], which we confirm by the direct lattice summation possible in two dimensions.

III. LUTTINGER-TISZA ANALYSIS

We first determine a ground state using the LT method [10] where it applies. Decomposing the interaction matrix into its Fourier components and denoting by $\lambda_{\min}(\mathbf{k})$ the lowest eigenvalue(s) of the interaction matrix, we use the fact that the energy of *any* spin configuration satisfies the bound,

$$H \geqslant N\lambda_{\min}(\mathbf{k}). \tag{7}$$

If there exists a spin configuration which can be decomposed into a linear combination of *only* the "optimal" [26] LT

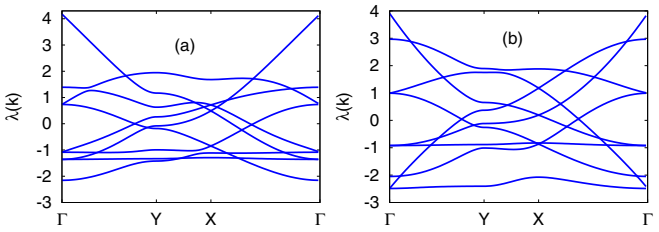

FIG. 2. (Color online) Eigenvalues of the interaction matrix $J_{ij}^{\alpha\beta}(\mathbf{k})$ along lines in the Brillouin zone. (a) Spectra for dominant exchange case $\theta = \pi/4$. (b) Spectra for $D = 1$, $\theta = 0$. The eigenvalue lowest in energy is generally at the Γ point $\mathbf{k}_0$.

eigenvectors corresponding to these eigenvalues, it is a global ground state. This happens if the "strong constraint" of unit length for the spins,

$$|\mathbf{S}_i|^2 = 1 \tag{8}$$

does not conflict with the optimal eigenvectors, which however in general have entries with different amplitudes. In the latter case, not unusual for non-Bravais lattices, nonoptimal modes have to be admixed, and the LT approach only yields an (often rather useful) guess at possible ground states or at least at leading instabilities from the high-temperature paramagnet.

A. Dominant AFM nearest-neighbor exchange

For pure nearest-neighbor antiferromagnetic exchange $\theta = \pi/2$ ($D = 0$), the lowest branch of the interaction matrix is exactly flat (dispersionless) reflecting the high ground-state degeneracy [27–30]. Decreasing θ we move to nonzero $D > 0$ which immediately lifts the degeneracy, selecting a ground state at wave vector $\mathbf{k}_0 = (0,0)$ as shown in Fig. 2(a) for $\theta = \pi/4$. The optimal eigenvector satisfies the constraint (8) and results in a 120° state which is doubly degenerate reflecting two possible chiralities. A further increase in D leads to level crossing at $\theta_1 = 10.01°$. Hence the 120° state is certainly stable up to this point as we have also confirmed in Monte Carlo simulations.

B. Dominant dipolar interactions or FM exchange

For $\theta < \theta_1$ LT no longer yields an exact ground state [31]. Instead, we enter an intermediate regime where neither spin-wave nor Monte Carlo computations (see Secs. V and VI) allow us reliably to conclude on the ground state. This regime persists up to the point $\theta_2 = 1.03°$ beyond which the 120° state is no longer even a stable local minimum at $\mathbf{k}_0 = (0,0)$.

For purely dipolar interactions $\theta = 0$ the minimal eigenvalue $\lambda_{\min} = -2.487$ is doubly degenerate and again occurs at $\mathbf{k}_0 = (0,0)$, Fig. 2(b). The best state we find has two of the spins that are inclined approximately by $\phi_{\approx} \pm 16°$ with respect to one of the unit-cell edges whereas the third spin remains unchanged (right panel of Fig. 1). This situation persists with varying $\phi(\theta)$ until the ferromagnetic point $\theta = -\pi/2$. However, in general no combination of the pair of eigenvectors satisfies the strong constraint on spin length (8). To determine the true ground state for hard unit length spins, we thus need to allow the admixing of other modes so that we next turn to numerics.

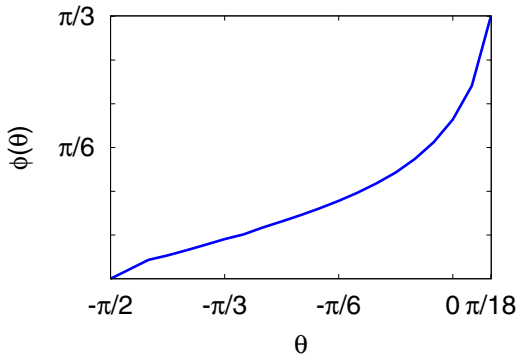

FIG. 3. (Color online) Inclination angle $\pm\phi$ of two of the spins in the unit cell (Fig. 1) as a function of θ [Eq. (4)] in the ferrimagnetic phase.

IV. NUMERICAL ENERGY MINIMIZATION FOR STRONG D OR FERROMAGNETIC J

Our Monte Carlo simulations (Sec. VI) do unveil a $\mathbf{k}_0 = (0,0)$ ordering at low temperatures, suggesting that hard spin constraint may optimally be satisfied by admixing higher modes at $\mathbf{k}_0 = (0,0)$ only. We therefore constrain our problem to a single unit cell and perform a numerical minimization of the Hamiltonian (5). The minimal energy configuration for the single unit cell is indeed the state found in full lattice Monte Carlo simulations. The ground state is a ferrimagnetic configuration in which the spins $\mathbf{S}_i$ take the following angles with one of the three edges in the unit cell:

$$\phi_1 = \phi, \quad \phi_2 = -\phi, \quad \phi_3 = 0,$$

with

$$\phi \approx 36.42° \tag{9}$$

for the pure dipolar interactions ($\theta = 0, J = 0$). As we change $-\pi/2 < \theta < \theta_2$ we can obtain a minimal energy ferrimagnetic configuration with a drifting $\phi(\theta)$ as shown in Fig. 3.

V. LINEAR SPIN-WAVE THEORY

We next study the role of quantum fluctuations around the two ground states discussed above. We find that both states are locally stable and exhibit a lowest band with little dispersion, in particular for the 120° state.

We evaluate the spin-wave spectrum of noncollinear spin structures using standard methods [32–34]. The Hamiltonian of a Bose gas of magnons reads

$$H = H^{(0)} + \sum_{\mathbf{k}} \sum_{i} \epsilon_i(\mathbf{k}) + \sum_{\mathbf{k}} \sum_{i} \epsilon_i(\mathbf{k})[a_i^\dagger(\mathbf{k}) a_i(\mathbf{k}) + a_i^\dagger(-\mathbf{k}) a_i(-\mathbf{k})], \tag{10}$$

where $a_i(\mathbf{k})$'s are boson annihilation operators with $H^{(0)}$ as the classical ground-state energy. For a stable ground-state spin configuration, H is Hermitian and all the spin-wave eigenenergies $\epsilon_i(\mathbf{k})$ are real. This yields the specific heat $C_v(T)$ and magnetization $M(T)$, allowing in principle for comparison with experimental data at low temperatures, e.g., below a scale set by the gap in the excitation spectrum [35].

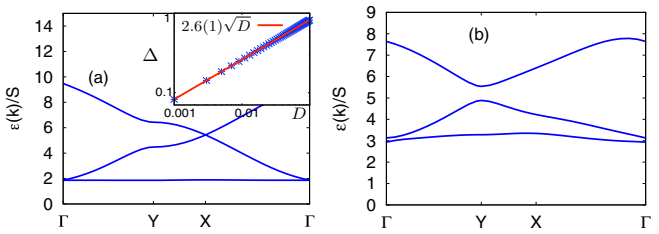

FIG. 4. (Color online) Spin-wave spectra for (a) the 120° state at $\theta = \pi/4$ and for (b) the ferrimagnetic ground state obtained by energy minimization at $\theta = 0$. In (a), the lowest branch remains almost perfectly flat while acquiring a gap $\propto \sqrt{D}$ (the inset).

We first confirm that the 120° and ferrimagnetic states at $\theta = \pi/4,0$, respectively, are stable to quantum fluctuations. Although it is known from previous studies [28] that for the 120° state the spin-wave excitation spectrum has a fully dispersionless (flat) band at zero energy as well as a twofold degenerate acoustic mode, the addition of D leads to a gap in the excitation spectrum proportional to $\sqrt{D}$ at small D. We plot the spin-wave spectra for cases $\theta = \pi/4$ and $\theta = 0$ in Fig. 4 where it is clearly seen that in both cases the leading effect of dipolar interactions is pushing the zero modes to finite frequency, expected on account of the absence of a continuous symmetry. The dispersion of the lowest branch of the 120° state is only weakly affected. This fact can manifest itself in finite energy almost **k**-independent resonance in inelastic neutron scattering [33,36]. The existence of the gap in the spectrum affects the corresponding specific heat and sublattice magnetization (Fig. 5). The gap leads to an exponential suppression of specific heat $C_v \sim \exp[-\Delta/T]$ or a reduction of staggered magnetization $\Delta M(T) \sim \exp[-\Delta/T]$ with the gap Δ.

Moreover we have checked for both $\theta = 0,\pi/4$ that these are the only stable spin-configurations at $\mathbf{k}_0 = (0,0)$. We close this section by noting that both the 120° and the ferrimagnetic states are locally stable within the boundaries of the intermediate phase (Fig. 1).

VI. MONTE CARLO SIMULATIONS

This section pursues two goals. First, the ground states are confirmed numerically; second, the corresponding finite-temperature phase transitions are analyzed in detail. This is performed with computationally intensive but tractable Monte Carlo simulations of the system on finite lattices with a linear dimension of $L \leqslant 24$ unit cells or $N \leqslant 1728$ sites.

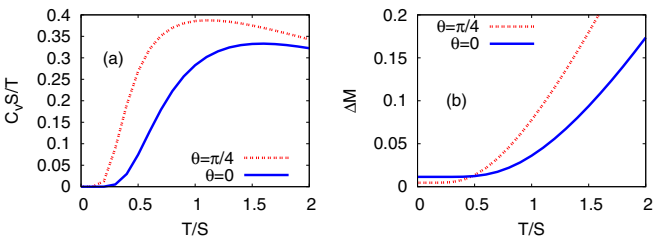

FIG. 5. (Color online) (a) Specific heat scaled by the temperature and (b) temperature dependence of the reduction of sublattice magnetization due to quantum fluctuations calculated using linear spin-wave theory, which is controlled in the limit of small T.

We employ parallel tempering with 64–128 replicas in the temperature range of $T = 0.125$–2.95 for the phase-transition analysis and in the range of $T = 0.00625$–2.95 to investigate the low-energy configuration of the dipoles. One Monte Carlo step corresponds to a sweep over the lattice in which on average every spin is touched. We perform $\approx 10^6$ Monte Carlo steps for the thermalization, followed by $\approx 10^6$ steps for every measuring round.

We obtain thermodynamic properties of the model (specific heat, uniform and staggered—120° state—magnetization, magnetic susceptibility, and fourth-order Binder cumulant) as well as the structure of the low-temperature spin configuration.

For the set of parameters leading to the ferrimagnetic ground state we analyze the phase transition via the behavior of the magnetic order parameter,

$$\mathbf{M} = \frac{1}{N}\sum_i \left(S_i^x, S_i^y, S_i^z\right), \tag{11}$$

where the sum is taken over all the sites in the lattice. For the planar 120° ground-state order we investigate the order parameter which captures the particular chiral spin pattern,

$$\mathbf{M}_\chi = \sqrt{\mathbf{m}_\chi \mathbf{m}_\chi^*}, \tag{12}$$

where

$$\mathbf{m}_\chi = \frac{1}{N}\sum_{\mathbf{R}+\mathbf{r}_j} \mathbf{S}(\mathbf{R}+\mathbf{r}_j)\exp(i\phi_j), \tag{13}$$

and ϕ_j are sublattice phase angles $\phi_1 = 0$, $\phi_2 = 2\pi/3$, and $\phi_3 = 4\pi/3$.

To investigate the corresponding finite-temperature phase transition we also compute the fourth-order Binder cumulant for the corresponding order parameter O given in Eq. (11) or (12),

$$U_L = 1 - \frac{1}{3}\frac{\langle O\rangle^4}{\langle O^2\rangle^2}, \tag{14}$$

as well as susceptibility,

$$\chi = \frac{N}{T}(\langle O^2\rangle - \langle O\rangle^2), \tag{15}$$

and specific heat per spin (see Figs. 6 and 7),

$$C/N = \frac{1}{N}\frac{1}{T^2}(\langle E^2\rangle - \langle E\rangle^2). \tag{16}$$

To characterize the phase transitions we employ standard finite-size scaling,

$$\begin{aligned} \tilde{M}(L^{1/\nu}t) &= L^{\beta/\nu}M_L, \\ \tilde{\chi}(L^{1/\nu}t) &= L^{-\gamma/\nu}\chi_L, \\ \tilde{C}(L^{1/\nu}t) &= L^{-\alpha/\nu}C_L, \end{aligned} \tag{17}$$

where $t = (T - T_c)/T_c$ is the reduced temperature. To obtain the critical exponent $1/\nu$ and critical point T_c we use the scaling

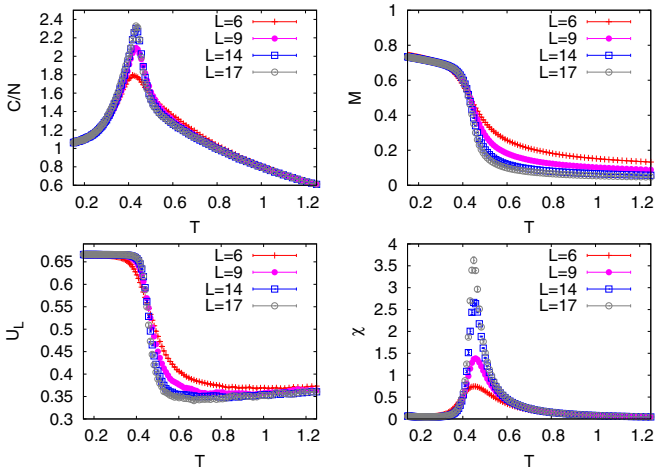

FIG. 6. (Color online) Monte Carlo results for specific heat C/N, Binder cumulant U_L, magnetization M, and susceptibility χ for $\theta = 0$ ($D = 1$ and $J = 0$).

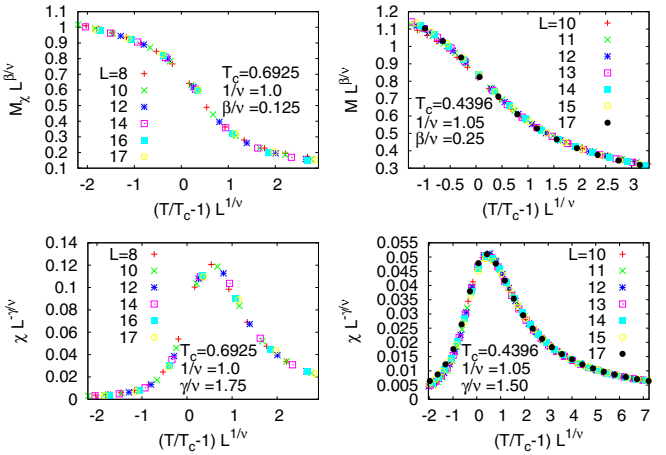

FIG. 8. (Color online) Scaling collapse for the magnetic (chiral) order parameter and its susceptibility for the transition into the 120° state (left) and the ferrimagnetic state (right).

relation for the Binder cumulant,

$$\tilde{U}(L^{1/\nu}t) = U_L. \tag{18}$$

We extract ν, β, α, γ, and T_c via data collapse.

Let us first look at the finite temperature transition to the 120° state. We perform MC simulations deep in the ordered phase for $\theta = 35.6°$. Collapsing the curves for chiral order parameter, Binder cumulant, susceptibility, and specific heat yields critical temperature T_c as well as the full set of critical exponents ν, β ,γ, and α see Fig. 8. The transition occurs at $T_c = 0.692(5)$, consistent with the 2D Ising universality class with critical exponents $\nu = 1$, $\beta = 1/8$, $\gamma = 7/4$, and $\alpha = 0$, reflecting the discrete Z_2 symmetry of the chiral order parameter.

For dominant dipolar interactions we analyze two points $\theta = 0$ and for $\theta = 1°$. The ferrimagnetic order has a sixfold discrete symmetry (the total spin of the triangular unit cell is collinear with one of its edges leading to the six possible

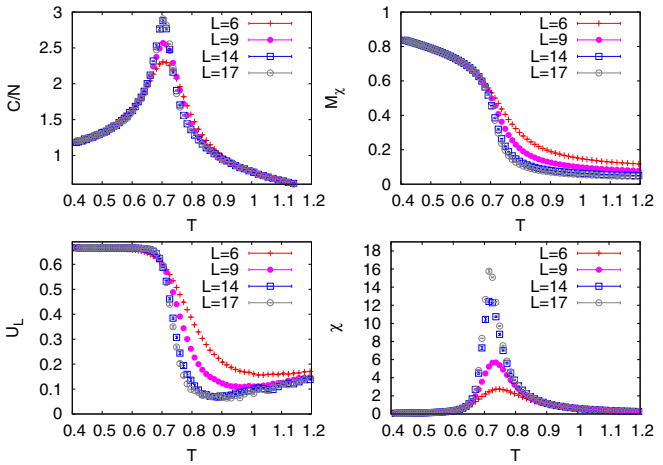

FIG. 7. (Color online) Monte Carlo results for specific heat C/N, Binder cumulant U_L, chiral order parameter M_χ, and corresponding susceptibility χ for $\theta = 35.6°$.

orientations) and at $T = 0$ differs only in the angle ϕ of the two inclined spins [Fig. 1(b)]. We therefore expect the corresponding transitions to belong to the same universality class.

Our Monte Carlo data show a clear divergence of the ferromagnetic order parameter, specific heat, and susceptibility as well as crossings of fourth-order Binder cumulant curves. This suggests a single second-order phase transition from a high-temperature paramagnet to a low-temperature ferrimagnetic phase (Fig. 6). Both for $\theta = 0°$ and $\theta = 1°$ we can extract critical temperatures $T_c = 0.439(2)$ and $T_c = 0.406(5)$ as well as the set of exponents which lead to the best data collapse of Binder cumulant, magnetization, susceptibility, and specific heat (Table I). Note that correlation length exponent ν and order parameter exponent β increase monotonically with J whereas the ratios $\beta/\nu \approx 0.25$ and $\gamma/\nu \approx 1.5$ remain constant with a two-dimensional scaling law implying $\eta = 2\beta/\nu \approx 0.5$.

This appears to provide an example of the so-called "weak universality" hypothesis which states that ratios of exponents should be independent of the details of the system Hamiltonian with $\eta = 2\beta/\nu$ and γ/ν universal whereas α and β are allowed to change [37]. The weak universality behavior is often observed as a drift from Berezinskii-Kosterlitz-Thoules (KT) exponents to discrete (i.e., Ising, Potts) transition exponents [38,39] and may of course be related to the existence of a large length scale. Note that in our case, we have a correspondence to a six-state clock model arising from a Hamiltonian with both nearest-neighbor and long-range interactions. Individually, a six-state clock model with only the former exhibits two KT transitions (not observed here) [40–43] whereas mean-field studies for the case of long-range dipolar

TABLE I. Critical exponents for the continuous phase transition analyzed with classical Monte Carlo.

	$1/\nu$	α/ν	β/ν	γ/ν	Universality class
$\theta \approx \pi/5$	1	0	1/8	7/4	Ising
$\theta = 0$	1.05(3)	0.10(3)	0.25(2)	1.5(2)	Unknown
$\theta = 1°$	1.17(3)	0.32(3)	0.25(3)	1.5(3)	Unknown

interactions suggest a single second-order low-temperature phase transition [44,45].

A low-temperature phase transition of pure dipoles on the kagome lattice was recently observed in the $O(N)$ Monte Carlo studies in Ref. [23]. The nature of the low-temperature spin arrangement was however not resolved due to the high computational cost of the $O(N)$ Monte Carlo algorithm inversely proportional to temperature. We have investigated the system at significantly lower temperatures where snapshots of the spin configurations give clear evidence of ferrimagnetic order at $\mathbf{k}_0 = (0,0)$. At the same time, the temperature dependence of the static structure factor does not indicate any intermediate ordering between the low-temperature ferrimagnetic state and the high-temperature disordered configuration. Together with our LT and spin-wave studies this rather strongly suggests that the ferrimagnetic $\mathbf{k} = (0,0)$ state is the low-temperature configuration of the dipoles.

In the intermediate regime between two three-sublattice phases (see Fig. 1) due to the existence of many metastable energy minima, our Monte Carlo simulations do not equilibrate even for our extensive parallel setup. We thus cannot provide a clear picture of physical quantities and leave a detailed investigation of this possibly incommensurate regime for future studies.

VII. DISCUSSION AND CONCLUSION

We have determined ground states, excitations, and phase transitions of classical Heisenberg spins with exchange and dipolar interactions on the frustrated kagome lattice.

Our first central result is a determination of the ground state for classical Heisenberg dipoles. This is a ferrimagnetic three-sublattice one. Note that dipolar interactions for Heisenberg spins lead to ground states in two-dimensional systems effectively confined on the plane of the lattice as a result of extensive energy cost of any finite out-of-plane component [3,13]. In our studies we indeed observe only in-plane spin states as the ground states of the model. Therefore, the ground states we find also apply to classical XY spins in the plane of the lattice.

Next, for the AFM nearest-neighbor exchange we observe that switching on a weak dipolar interaction lifts the extensive ground-state degeneracy of the nearest-neighbor model which exists here as it does in many other frustrated lattices, e.g., the Archimedean pyrochlore lattice in three dimensions [46,47]. In both cases, the elementary simplices—triangles for kagome, tetrahedra for pyrochlore—have a vanishing total dipole moment in the nearest-neighbor ground state; upon adding dipolar interactions, they enter a state where the quadrupole moment of each simplex also vanishes [48]. However, for stronger values of the dipolar interaction, the suppression of the leading multipole moment no longer seems to be favorable. The general principles governing the low-energy states on individual clusters [49] and how they combine to form a large lattice is an intriguing topic for future studies.

The concomitant line of phase transitions into the ferrimagnetic state at various D's appears to have exponents ν and β change monotonically with the ratios β/ν and γ/ν constant. This is known in the context of the weak universality hypothesis and often appears in systems with n-fold anisotropy where exponents appear to drift from KT values to those of discrete continuous transitions. The presence of an enigmatic slice of the phase diagram where our methods fail to produce a reliable answer further focuses attention on the possibility of the appearance of incommensurate states for delicately balanced exchange and dipolar interactions.

Moreover, it seems rather remarkable that the flat band of zero-energy excitations simply moves up in energy without acquiring almost any dispersion. We do note that this phenomenon is not so uncommon, after all, with a range of different perturbations capable of producing a similar phenomenon, a case in point being magnetoelastic interactions [50]. Also, a recent preprint [51] noted the same phenomenon for a dipolar magnet on the gadolinium gallium garnet (GGG) lattice, which has historically played an immensely important role in the experimental study of frustrated magnetic materials. This may very well be one of the best experimental handles on dipolar interactions, leading to an almost $\mathbf{k}$-independent resonance in inelastic neutron scattering [33,36] at a nonzero energy scaling quite sensitively with the size of the dipolar interaction $\sim\sqrt{D}$.

The prospect for experimental work in this field is probably better now than it has been for a very long time. In a large number of systems the role of dipolar interactions is important or even dominant [2,9,52,53]. There is significant progress in fabrication of dipolar nanoarrays with a complex frustrated lattice geometry [54,55] as well as recent progress on building a dipolar system in optical lattices [4,56]. In addition recent progress in fabricating thin films of frustrated materials [57,58] suggests a possible route for the realization of dipolar films with a kagome geometry. Here the possible candidates for a film realization could be fcc kagome materials $RhMn_3$, $PtMn_3$, and $IrMn_3$ [59,60] where the latter one is commonly used in thin-film technology [61,62]. $RhMn_3$ and $PtMn_3$ have the fcc crystal structure [63–65] where magnetic Mn ions reside on the cube faces and the nonmagnetic (Ir) ions site at the cube corners. The magnetic ions can thus be viewed as being on ABC stacked (111) kagome planes where each site has eight NN's (four in plane, two to the plane above, and two to the plane below). The (111) plane is perpendicular to the film plane in thin-film applications, and thus one deals with a thin stack of L kagome layers. Interestingly the bulk of $IrMn_3$ exhibits a long-range magnetic order below $T_N \approx 960$ K [60] which is the three-dimensional manifestation of the 120° $q = 0$ spin structure [66] one of the structures found in our studies to be stabilized by weak dipolar interactions. Similar magnetic order is also found in $RhMn_3$ and $PtMn_3$.

We hope that our work will provide motivation for a detailed characterization of the nature and collective behavior of some of these experimental systems.

ACKNOWLEDGMENTS

We are grateful to P. Deen, P. A. McClarty, J. Richter, L. Seabra, and R. Valenti for useful discussions. We thank Rechenzentrum Garching (RZG) for computing time for the parallel simulations. M.M. acknowledges ICMP of NAS of Ukraine (Lviv) where part of the initial computations was performed. We acknowledge funding by the DFG via SFB 1143.

APPENDIX: LINEAR SPIN-WAVE THEORY

Our spin-wave analysis in the noncollinear magnetic systems starts with a rotation from the global z direction to the local frame for each moment. Let $\tilde{\mathbf{S}}_i(\mathbf{R}^k)$ point along its local z axis so that it is related to the spin operator defined in the crystallographic frame via the rotation,

$$\mathbf{S}_i(\mathbf{R}^k) = \mathbb{R}_i^{-1}\tilde{\mathbf{S}}_i(\mathbf{R}^k), \tag{A1}$$

where $\mathbb{R}_i$ is the corresponding rotation matrix. In the local frame the Hamiltonian reads

$$H = -\frac{1}{2}\sum_{i,j}\sum_{\alpha,\beta}\sum_{k,l}\mathcal{J}_{ij}^{\alpha\beta}\left(\mathbf{R}_{ij}^{kl}\right)\tilde{S}_i^{\alpha}(\mathbf{R}^k)\tilde{S}^{\beta}{}_j(\mathbf{R}^l), \tag{A2}$$

where the interaction matrix components transform as

$$\mathcal{J}_{ij}\left(\mathbf{R}_{ij}^{kl}\right) = \mathbb{R}_i^{-1}J_{ij}\left(\mathbf{R}_{ij}^{kl}\right)\mathbb{R}_j. \tag{A3}$$

Fourier transforming spin operators and the interaction matrix gives

$$\tilde{S}_i^{\alpha}(\mathbf{R}^k) = \frac{1}{\sqrt{N}}\sum_{\mathbf{k}}\tilde{S}_i^{\alpha}(\mathbf{k})\exp[ik\cdot(\mathbf{R}^k+\mathbf{r}_i)], \tag{A4}$$

$$\mathcal{J}_{ij}^{ij}(\mathbf{k}) = \sum_{kl}\mathcal{J}_{ij}^{ij}\left(\mathbf{R}_{ij}^{kl}\right)\exp\left[-i\mathbf{k}\cdot\mathbf{R}_{ij}^{kl}\right], \tag{A5}$$

where N is the number of underlying Bravais lattice points. Thus, the Hamiltonian in reciprocal space is

$$H = -\frac{1}{2}\sum_{i,j}\sum_{\alpha,\beta}\sum_{\mathbf{k}}\tilde{S}_i^{\beta}(\mathbf{k})\mathcal{J}_{ij}^{ij}(\mathbf{k})\tilde{S}^{\beta}{}_j(-\mathbf{k}). \tag{A6}$$

The linearized Holstein-Primakoff transformation then gives

$$\begin{aligned}
\tilde{S}_i^x(\mathbf{k}) &= \sqrt{\frac{S}{2}}[c_i^{\dagger}(\mathbf{k}) + c_i(-\mathbf{k})],\\
\tilde{S}_i^y(\mathbf{k}) &= i\sqrt{\frac{S}{2}}[c_i^{\dagger}(\mathbf{k}) - c_i(-\mathbf{k})],\\
\tilde{S}_i^z(\mathbf{k}) &= \sqrt{N}S\delta_{\mathbf{k},0}\exp[-i\mathbf{k}\cdot\mathbf{r}_i] - \frac{1}{\sqrt{N}}\sum_{\mathbf{k}'}c_i^{\dagger}(\mathbf{k}')c_i(\mathbf{k}'-\mathbf{k}),
\end{aligned} \tag{A7}$$

with boson operators $[c_i(\mathbf{k}),\, c_j^{\dagger}(\mathbf{k}')] = \delta_{i,j}\delta_{\mathbf{k},\mathbf{k}'}$. Keeping only terms up to second order, we obtain

$$H = H^{(0)} + H^{(1)} + H^{(2)}, \tag{A8}$$

where

$$\begin{aligned}
H^{(0)} &= -\frac{1}{2}NS^2\sum_{i,j}\mathcal{J}_{ij}^{zz}(0),\\
H^{(1)} &= -S\sqrt{\frac{NS}{2}}\sum_{i,j}[F_{ij}(0)c_i^{\dagger}(0) + F_{ij}^{\star}(0)c_i^{\dagger}(0)],
\end{aligned} \tag{A9}$$

$$\begin{aligned}
H^{(2)} = -\frac{1}{2}S\sum_{i,j}\sum_{\mathbf{k}}[&A_{ij}(\mathbf{k})c_i^{\dagger}(\mathbf{k})c_j(\mathbf{k}) + B_{ij}(\mathbf{k})c_i^{\dagger}(\mathbf{k})c_j^{\dagger}(-\mathbf{k})\\
&+B_{ij}^{\star}(\mathbf{k})c_i(-\mathbf{k})c_j(\mathbf{k}) + A_{ij}^{\star}(\mathbf{k})c_i(-\mathbf{k})c_j^{\dagger}(-\mathbf{k})],
\end{aligned}$$

and

$$\begin{aligned}
F_{ij}(0) &= \mathcal{J}_{ij}^{xz}(0) + i\mathcal{J}_{ij}^{yz}(0),\\
A_{ij}(\mathbf{k}) &= \frac{1}{2}\left\{\mathcal{J}_{ij}^{xx}(\mathbf{k}) + \mathcal{J}_{ij}^{yy}(\mathbf{k}) - i\left[\mathcal{J}_{ij}^{xy}(\mathbf{k}) - \mathcal{J}_{ij}^{yx}(\mathbf{k})\right]\right\}\\
&\quad - \sum_{\gamma}\mathcal{J}_{i\gamma}^{zz}(0)\delta_{i,j},\\
B_{ij}(\mathbf{k}) &= \frac{1}{2}\left\{\mathcal{J}_{ij}^{xx}(\mathbf{k}) - \mathcal{J}_{ij}^{yy}(\mathbf{k}) + i\left[\mathcal{J}_{ij}^{xy}(\mathbf{k}) + \mathcal{J}_{ij}^{yx}(\mathbf{k})\right]\right\}.
\end{aligned} \tag{A10}$$

The equilibrium condition that on every site the effective magnetic field be parallel to the spin direction implies the absence of linear terms. This is satisfied if $\sum_j F_{ij}(0) = 0$. If the spin ground state is stable after the canonical transformation the Hamiltonian can be written in diagonal form

$$\begin{aligned}
H = H^{(0)} &+ \sum_{\mathbf{k}}\sum_{i}\epsilon_i(\mathbf{k})\\
&+ \sum_{\mathbf{k}}\sum_{i}\epsilon_i(\mathbf{k})[a_i^{\dagger}(\mathbf{k})a_i(\mathbf{k}) + a_i^{\dagger}(-\mathbf{k})a_i(-\mathbf{k})],
\end{aligned} \tag{A11}$$

where $a_i(\mathbf{k})$ and $a_i^{\dagger}(\mathbf{k})$ are new boson operators and all the eigenenergies $\epsilon_i(\mathbf{k})$ are real.

The specific heat is

$$C_v = \frac{\beta^2}{N}\sum_{\mathbf{k}}\sum_{i}\{\epsilon_i(\mathbf{k})n_{\mathrm{B}}[\epsilon_i(\mathbf{k})]\}^2\exp[\beta\epsilon_i(\mathbf{k})], \tag{A12}$$

where $n_{\mathrm{B}}[\epsilon_i(\mathbf{k})] = [\epsilon_i(\mathbf{k}) - 1]^{-1}$ is a Bose factor. The sublattice magnetization $M(T)$ is obtained by taking into account the role of quantum and thermal fluctuations,

$$M(T) = S - \Delta S - \frac{1}{N}\sum_{\mathbf{k}}\sum_{i}[Q^{\dagger}Q]_{ii}n_{\mathrm{B}}[\epsilon_i(\mathbf{k})], \tag{A13}$$

where

$$\Delta S = \frac{1}{2}\left(\frac{1}{N}\sum_{\mathbf{k}}\sum_{i}[Q^{\dagger}Q]_{ii} - 1\right) \tag{A14}$$

is the zero-temperature reduction of classical spin polarization and Q is the matrix diagonalizing the spin-wave Hamiltonian.

[1] J. S. Gardner, M. J. P. Gingras, and J. E. Greedan, Rev. Mod. Phys. **82**, 53 (2010).

[2] C. Nisoli, R. Moessner, and P. Schiffer, Rev. Mod. Phys. **85**, 1473 (2013).

[3] K. De'Bell, A. B. MacIsaac, and J. P. Whitehead, Rev. Mod. Phys. **72**, 225 (2000).

[4] G. Pupillo, A. Micheli, H. Büchler, and P. Zoller, in *Cold Molecules: Theory, Experiment, Applications*, edited by R. V. Krems, W. C. Stwalley, and B. Friedrich (CRC, Boca Raton, FL, 2009).

[5] D. Peter, S. Müller, S. Wessel, and H. P. Büchler, Phys. Rev. Lett. **109**, 025303 (2012).

[6] R. Moessner, Can. J. Phys. **79**, 1283 (2001).
[7] S. T. Bramwell and M. J. Gingras, Science **294**, 1495 (2001).
[8] R. Moessner and S. L. Sondhi, Phys. Rev. Lett. **105**, 166401 (2010).
[9] C. Castelnovo, R. Moessner, and S. L. Sondhi, Nature (London) **451**, 42 (2008).
[10] J. M. Luttinger and L. Tisza, Phys. Rev. **70**, 954 (1946).
[11] J. Brankov and D. Danchev, Physica A (Amsterdam) **144**, 128 (1987).
[12] V. Rozenbaum and V. Ogenko, JETP Lett. **35**, 184 (1982).
[13] S. V. Maleev, Sov. Phys. JETP **43**, 1240 (1976).
[14] S. Prakash and C. L. Henley, Phys. Rev. B **42**, 6574 (1990).
[15] J. F. Fernández and J. J. Alonso, Phys. Rev. B **76**, 014403 (2007).
[16] P. I. Belorobov, R. S. Gekht, and V. A. Ignatchenko, Sov. Phys. JETP **57**, 636 (1983).
[17] E. Rastelli, S. Regina, and A. Tassi, Phys. Rev. B **67**, 094429 (2003).
[18] P. Politi, M. G. Pini, and R. L. Stamps, Phys. Rev. B **73**, 020405 (2006).
[19] D. Danchev, Physica A (Amsterdam) **163**, 835 (1990).
[20] J. Sasaki and F. Matsubara, J. Phys. Soc. Jpn. **67**, 1134 (1998).
[21] S. Yan, D. A. Huse, and S. R. White, Science **332**, 1173 (2011).
[22] G.-W. Chern and R. Moessner, Phys. Rev. Lett. **110**, 077201 (2013).
[23] Y. Tomita, J. Phys. Soc. Jpn. **78**, 114004 (2009).
[24] J. Richter, J. Schulenburg, and A. Honecker, *Quantum Magnetism* (Springer, Berlin, 2004), pp. 85–153.
[25] M. Enjalran and M. J. P. Gingras, Phys. Rev. B **70**, 174426 (2004).
[26] M. F. Lapa and C. L. Henley, arXiv:1210.6810.
[27] J. T. Chalker, P. C. W. Holdsworth, and E. F. Shender, Phys. Rev. Lett. **68**, 855 (1992).
[28] A. B. Harris, C. Kallin, and A. J. Berlinsky, Phys. Rev. B **45**, 2899 (1992).
[29] I. Ritchey, P. Chandra, and P. Coleman, Phys. Rev. B **47**, 15342 (1993).
[30] D. A. Huse and A. D. Rutenberg, Phys. Rev. B **45**, 7536 (1992).
[31] In this region we also observe a shift in optimal wave vector $\mathbf{k}_0$ to the Y point if $\theta_1 < \theta < \theta_Y$, where $\theta_Y = 9.77^\circ$.
[32] R. White, M. Sparks, and I. Ortenburger, Phys. Rev. **139**, A450 (1965).
[33] A. G. D. Maestro and M. J. P. Gingras, J. Phys.: Condens. Matter **16**, 3339 (2004).
[34] J. Colpa, Physica A (Amsterdam) **93**, 327 (1978).
[35] J. A. Quilliam, K. A. Ross, A. G. Del Maestro, M. J. P. Gingras, L. R. Corruccini, and J. B. Kycia, Phys. Rev. Lett. **99**, 097201 (2007).
[36] S.-H. Lee, C. Broholm, T. H. Kim, W. Ratcliff, and S. W. Cheong, Phys. Rev. Lett. **84**, 3718 (2000).
[37] M. Suzuki, Prog. Theor. Phys. **51**, 1992 (1974).
[38] L. Seabra, T. Momoi, P. Sindzingre, and N. Shannon, Phys. Rev. B **84**, 214418 (2011).
[39] A. Taroni, S. T. Bramwell, and P. C. Holdsworth, J. Phys.: Condens. Matter **20**, 275233 (2008).
[40] M. S. S. Challa and D. P. Landau, Phys. Rev. B **33**, 437 (1986).
[41] S. Fujiki and T. Horiguchi, J. Phys. Soc. Jpn. **64**, 1293 (1995).
[42] J. Tobochnik, Phys. Rev. B **26**, 6201 (1982).
[43] J. V. José, L. P. Kadanoff, S. Kirkpatrick, and D. R. Nelson, Phys. Rev. B **16**, 1217 (1977).
[44] S.-T. Chen, Phys. Lett. A **168**, 140 (1992).
[45] S.-T. Chen, Phys. Lett. A **176**, 149 (1993).
[46] R. Moessner and J. T. Chalker, Phys. Rev. B **58**, 12049 (1998).
[47] R. Moessner and J. T. Chalker, Phys. Rev. Lett. **80**, 2929 (1998).
[48] S. E. Palmer and J. T. Chalker, Phys. Rev. B **62**, 488 (2000).
[49] J. Schönke, T. M. Schneider, and I. Rehberg, Phys. Rev. B **91**, 020410 (2015).
[50] O. Tchernyshyov, R. Moessner, and S. L. Sondhi, Phys. Rev. Lett. **88**, 067203 (2002).
[51] N. d'Ambrumenil, O. A. Petrenko, H. Mutka, and P. P. Deen, arXiv:1501.03493.
[52] I. Szalai and S. Dietrich, Eur. Phys. J. E **28**, 347 (2009).
[53] V. Rozenbaum, V. M. Ogenko, and A. Chuiko, Phys.-Usp. **34**, 883 (1991).
[54] R. F. Wang, C. Nisoli, R. S. Freitas, J. Li, W. McConville, B. J. Cooley, M. S. Lund, N. Samarth, C. Leighton, V. H. Crespi, and P. Schiffer, Nature (London) **439**, 303 (2006).
[55] G. Möller and R. Moessner, Phys. Rev. Lett. **96**, 237202 (2006).
[56] N. Y. Yao, C. R. Laumann, A. V. Gorshkov, S. D. Bennett, E. Demler, P. Zoller, and M. D. Lukin, Phys. Rev. Lett. **109**, 266804 (2012).
[57] D. Leusink, F. Coneri, M. Hoek, S. Turner, H. Idrissi, G. Van Tendeloo, and H. Hilgenkamp, APL Mater. **2**, 032101 (2014).
[58] M. S. Bhuiyan, M. Paranthaman, S. Sathyamurthy, A. Goyal, and K. Salama, J. Mater. Res. **20**, 904 (2005).
[59] M. D. LeBlanc, M. L. Plumer, J. P. Whitehead, and B. W. Southern, Phys. Rev. B **88**, 094406 (2013).
[60] I. Tomeno, H. N. Fuke, H. Iwasaki, M. Sahashi, and Y. Tsunoda, J. Appl. Phys. **86**, 3853 (1999).
[61] M. Tsunoda, H. Takahashi, and M. Takahashi, IEEE Trans. Magn. **45**, 3877 (2009).
[62] M. Tsunoda, H. Takahashi, T. Nakamura, C. Mitsumata, S. Isogami, and M. Takahashi, Appl. Phys. Lett. **97**, 072501 (2010).
[63] E. Krén, G. Kádár, L. Pál, J. Sólyom, and P. Szabó, Phys. Lett. **20**, 331 (1966).
[64] A. Sakuma, R. Y. Umetsu, and K. Fukamichi, Phys. Rev. B **66**, 014432 (2002).
[65] T. Ikeda and Y. Tsunoda, J. Phys. Soc. Jpn. **72**, 2614 (2003).
[66] V. Hemmati, M. L. Plumer, J. P. Whitehead, and B. W. Southern, Phys. Rev. B **86**, 104419 (2012).